

${}^6\text{He}$ -triton cluster states in ${}^9\text{Li}$

Yoshiko Kanada-En'yo

Department of Physics, Kyoto University, Kyoto 606-8502, Japan

Tadahiro Suhara

Yukawa Institute for Theoretical Physics, Kyoto University, Kyoto 606-8502, Japan

Cluster states in ${}^9\text{Li}$ are investigated with calculations of a ${}^6\text{He}$ - t cluster model. Results suggest ${}^6\text{He}$ - t cluster states near the ${}^6\text{He}$ - t threshold energy. These states construct a $K^\pi = 1/2^-$ band and their neutron configuration is similar to that of the $K^\pi = 0_2^+$ band in ${}^{10}\text{Be}$.

I. INTRODUCTION

It has been revealed that cluster structures appear in light unstable nuclei as well as light stable nuclei. In the recent progress of experimental and theoretical researches on unstable nuclei, various exotic cluster states have been discovered in neutron-rich nuclei where valence neutrons play an important role.

For instance, a variety of cluster structures have been found in neutron-rich Be isotopes. Many of low-lying states of Be isotopes are understood in a molecular orbital picture where a Be nucleus is considered to consist of 2 α 's and valence neutron(s) in molecular orbitals around the 2α core [1–13]. In highly excited states near the He+He threshold energy of ${}^{10}\text{Be}$ and ${}^{12}\text{Be}$, well-developed cluster states have been suggested experimentally and theoretically [7, 12–20]. Those developed cluster states show two-body cluster structures such as ${}^6\text{He}+{}^4\text{He}$ in ${}^{10}\text{Be}$ and ${}^6\text{He}+{}^6\text{He}$ in ${}^{12}\text{Be}$. Also in the neighboring nuclei, ${}^{14}\text{Be}$ and ${}^{15}\text{B}$, developed two-body cluster states at high excitation energy have been suggested theoretically [21].

Excitation energies of those developed two-body cluster states in neutron-rich nuclei can be understood systematically from the point of view of Ikeda's threshold rule which suggests appearances of developed cluster states near the corresponding threshold energy [22]. From the Ikeda's threshold rule, we expect possible appearance of ${}^6\text{He}+t$ cluster states near the ${}^6\text{He}+t$ threshold energy in excited states of ${}^9\text{Li}$. It is a challenging issue in physics of unstable nuclei to search for such resonances of two neutron-rich clusters.

In our previous study with the quadrupole deformation (β - γ) constraint in a framework of antisymmetrized molecular dynamics (AMD), we have shown an indication of a largely deformed state having a ${}^6\text{He}+t$ structure in excited states of ${}^9\text{Li}$ [23]. The energy surface on the β - γ plane shows a shallow local minimum in the large prolate region. The intrinsic wave function at the local minimum has a developed ${}^6\text{He}+t$ cluster feature and it shows an elongate prolate shape of the neutron density which is analogous to the neutron structure of the ${}^{10}\text{Be}(0_2^+)$ having a developed ${}^6\text{He}+{}^4\text{He}$ cluster feature. Note that the ${}^6\text{He}+t$ and ${}^6\text{He}+{}^4\text{He}$ cluster structures in these states are not weak-coupling cluster states but rather strong coupling ones where a t or a ${}^4\text{He}$ cluster is sitting on the head

of a deformed ${}^6\text{He}$ cluster. According to the previous calculation, the excitation energy of the ${}^6\text{He}+t$ cluster state in ${}^9\text{Li}$ is expected to be 2 MeV higher than that of the ${}^{10}\text{Be}(0_2^+)$, and hence, it might be a state above the ${}^6\text{He}+t$ threshold.

To investigate ${}^6\text{He}+t$ -cluster states near the ${}^6\text{He}+t$ threshold in ${}^9\text{Li}$, we perform GCM calculations with a ${}^6\text{He}+t$ cluster model. We first show the energy levels and $E2$ strengths obtained by the GCM calculations in a bound state approximation. Then we discuss stability and spectra of the resonances by an analysis using a pseudo potential method.

This paper is organized as follows. In section II, we explain the formulation of the present calculations. We show the calculated results in section III and finally give a summary in section IV.

II. FORMULATION

To incorporate ${}^6\text{He}+t$ resonance features, we use Bloch-Brink (BB) [24] ${}^6\text{He}+t$ cluster wave functions having various inter-cluster distances and superpose them. The ${}^6\text{He}$ and t cluster wave functions are written by harmonic oscillator (HO) shell-model wave functions localized at $(0, 0, -d/3)$ and $(0, 0, +2d/3)$, respectively. Here d indicates the distance parameter, which is treated as a generator coordinate in the superposition. The width parameter $\nu = 1/2b^2$ is common for ${}^6\text{He}$ and t clusters.

A t cluster is given by the $(0s)_\pi(0s)_\nu^2$ configuration shell-model wave function. A configuration for a ${}^6\text{He}$ cluster is assumed to be $(0s)_\pi^2(0s)_\nu^2(0p)_\nu^2$ which indicates an α cluster and two valence neutrons in p shell. For p -shell neutron configurations, we choose $(p_{3/2})^2$ coupling to the total angular momentum $J_{12} = 0, 2$ in the j - j coupling scheme, and also the total intrinsic spin $S_{12} = 0$ configurations in the l - s coupling scheme. Namely, the neutron configurations are given by $|p_z, n \uparrow\rangle|p_z, n \downarrow\rangle$ and $|p_{(+)}, n \uparrow\rangle|p_{(-)}, n \downarrow\rangle$, and their rotated states. Here $p_{(+)}, p_z, p_{(-)}$ stand for $l_z = +1, 0, -1$ (z -component of orbital angular momentum) states in p shell, respectively.

Then, the ${}^6\text{He}+t$ cluster wave functions projected onto parity and total-angular-momentum eigen states are

written as,

$$P_{MK}^{J\pm}|\Phi_{\tau}(d)\rangle = P_{MK}^{J\pm}\mathcal{A}\left\{|\psi_{1\tau}(-\frac{d}{3})\rangle|\psi_{2\tau}(-\frac{d}{3})\rangle\right. \\ \times |\phi(-\frac{d}{3})p\uparrow\rangle|\phi(-\frac{d}{3})p\downarrow\rangle|\phi(-\frac{d}{3})n\uparrow\rangle|\phi(-\frac{d}{3})n\downarrow\rangle \\ \left.\times |\phi(\frac{2d}{3})p\uparrow\rangle|\phi(\frac{2d}{3})n\uparrow\rangle|\phi(\frac{2d}{3})n\downarrow\rangle\right\}. \quad (1)$$

Here $\phi(-d/3)$ and $\phi(2d/3)$ are shifted 0s wave functions localized at $(0, 0, -d/3)$ and $(0, 0, 2d/3)$, respectively. $|\psi_{1\tau}(-\frac{d}{3})\rangle$ and $|\psi_{2\tau}(-\frac{d}{3})\rangle$ indicate single-particle states for two valence neutrons, and given by the p -shell orbits shifted at $(0, 0, -d/3)$. Six configurations labeled by $\tau = \{a, b, c, d, e, f\}$, which are illustrated in Fig. 1, are used to describe valence neutron configurations of a ${}^6\text{He}$ cluster. In the configuration $\tau = a$, two neutron orbitals $|\psi_{1a}(-d/3)\rangle$ and $|\psi_{2a}(-d/3)\rangle$ are chosen to be $|p_z, n\uparrow\rangle_{-d/3}$ and $|p_z, n\downarrow\rangle_{-d/3}$ that are p orbits around $(0, 0, -d/3)$. We define a rotational operator $R(\theta, -d/3)$ for the rotation around the point $(0, 0, -d/3)$ with respect to the vector $(1, 0, 0)$. Then, two neutron orbitals for the configurations (b) and (c) can be written as

$$|\psi_{1\tau}(-d/3)\rangle = R(\theta, -d/3)|p_z, n\uparrow\rangle_{-d/3}, \quad (2)$$

$$|\psi_{2\tau}(-d/3)\rangle = R(\theta, -d/3)|p_z, n\downarrow\rangle_{-d/3}, \quad (3)$$

with $\theta = \pi/4$ and $\theta = \pi/2$, respectively. Similarly, two neutrons orbitals for the configuration (f) are

$$|\psi_{1f}(-d/3)\rangle = |p_{(+)}, n\uparrow\rangle_{-d/3}, \quad (4)$$

$$|\psi_{2f}(-d/3)\rangle = |p_{(-)}, n\downarrow\rangle_{-d/3}, \quad (5)$$

and those for the configurations (d) and (e) can be written as

$$|\psi_{1\tau}(-d/3)\rangle = R(\theta, -d/3)|p_{(+)}, n\uparrow\rangle_{-d/3}, \quad (6)$$

$$|\psi_{2\tau}(-d/3)\rangle = R(\theta, -d/3)|p_{(-)}, n\downarrow\rangle_{-d/3}, \quad (7)$$

with $\theta = \pi/2$ and $\theta = \pi/4$, respectively. Configurations (a), (b), and (c) correspond to $|L_{12} = 0, 2\rangle \otimes |S_{12} = 0\rangle$ states of a ${}^6\text{He}$ cluster in the l - s coupling scheme, while (d), (e), and (f) indicate the $(p_{3/2})^2$ configurations of a ${}^6\text{He}$ cluster in the j - j coupling scheme. Here L_{12} stands for the magnitude of total orbital angular momentum of two valence neutrons. The projected ${}^6\text{He}+t$ cluster wave functions for these six configurations cover all 0^+ and 2^+ states in p -shell configurations of a ${}^6\text{He}$ cluster and spin-up and spin-down configurations for a triton cluster.

We suppose ${}^6\text{He}-t$ cluster wave functions,

$$|\Psi_M^{Jk\pm}\rangle = \sum_d \sum_{\tau, K} c_{d, \tau, K}^{(k)} P_{MK}^{J\pm} |\Phi_{\tau}(d)\rangle, \quad (8)$$

where coefficients are determined by diagonalizing norm and Hamiltonian matrices. This corresponds to a calculation of a generator coordinate method GCM with the generator coordinate d .

We can also perform a GCM calculation for ${}^{10}\text{Be}$ with a ${}^6\text{He}+\alpha$ cluster model in a similar way by replacing a t cluster with an α cluster.

As already mentioned, the cluster structures suggested in ${}^9\text{Li}$ and ${}^{10}\text{Be}$ near the ${}^6\text{He}+t$ and ${}^6\text{He}+{}^4\text{He}$ threshold energies may be not weak-coupling cluster states but contain strong coupling cluster components where the inter-cluster motion couples strongly to the orientation of a deformed ${}^6\text{He}$ cluster, i.e., valence neutron configurations. In preceding works [3–10, 18], the $K^{\pi} = 0_2^+$ band of ${}^{10}\text{Be}$ is considered to be a molecular orbital state having two valence neutrons in the molecular σ orbital around the 2α cluster core. In the case that α - α distance is moderate, the configuration (a) in Fig. 1 corresponds to the molecular orbital σ^2 state as the valence neutron orbital has a nodal structure along the z -axis due to the antisymmetrization with neutrons in α clusters, and it is nothing but the strong coupling cluster structure. On the other hand, in the asymptotic region that the inter-cluster distance is far enough, a two-cluster system should become a weak coupling state where a ${}^6\text{He}$ cluster has a certain spin and parity J^{π} which weakly couple with inter-cluster motion. In the present framework, the transition between the strong coupling regime to the weak coupling regime is taken into account by the linear combination of configurations (a)-(f) projected onto the total angular momentum eigen states.

Practically, we express a configuration of a BB wave function by using a single AMD wave function which is given by a Slater determinant of single-particle Gaussian wave packets. A general form of AMD wave functions is described, for example, in Refs. [11, 25].

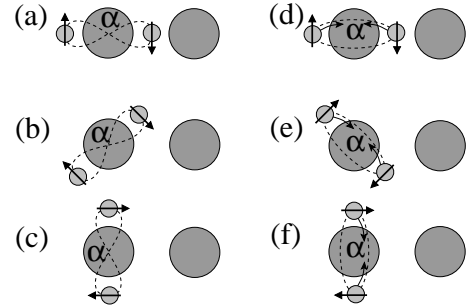


FIG. 1: Schematic figures for configurations (a)-(f) of a ${}^6\text{He}$ cluster in the BB ${}^6\text{He}+t$ and ${}^6\text{He}+\alpha$ cluster models.

III. RESULTS

A. Effective nuclear forces and parameters

The effective Hamiltonian is

$$H_{\text{eff}} = \sum_i t_i + \sum_{i < j} v_{ij}, \quad (9)$$

where the first term is kinetic term and the second term for two-body interactions consists of effective nuclear forces and Coulomb force. The adopted effective nuclear forces are the Volkov No.2 force [26] for finite-range central force and the spin-orbit term of the G3RS force [27] for spin-orbit force. These nuclear forces have been used in many works on structures of ^{10}Be and ^9Li [6, 8, 23]. The interaction parameters are ($b = h = 0.125, m = 0.60$) for the Volkov No.2 force and $u_I = -u_{II} = 1600$ MeV for the strength of the spin-orbit force. These are the same as those used in Refs. [23, 28]. Coulomb force is approximated by seven-range Gaussians.

As for the width parameter ν of the HO shell-model wave functions for ^6He , t , and ^4He clusters, the parameter $\nu = 0.235 \text{ fm}^{-2}$ used in Refs. [23, 28] is adopted. The generator coordinate d in the GCM calculations is taken to be $d = 1, 2, \dots, 8$ fm. The truncation of the coordinate $d \leq 8$ fm in the GCM calculation corresponds to a bound-state approximation. To see resonance features and coupling with continuum states, we also take a larger model space, $d = 1, 2, \dots, 15$ fm.

B. Energy levels of ^9Li and ^{10}Be

We superpose the $^6\text{He}+t$ cluster wave functions with $d = 1, 2, \dots, 8$ fm and obtain energy levels of ^9Li . The calculated energy and $^6\text{He}+t$ threshold energy are -34.3 and -26.0 MeV, respectively. Though the calculations overestimate the experimental energy (-45.3 MeV) and the threshold energy (-37.8 MeV), they reproduce well the ^9Li energy relative to the $^6\text{He}+t$ threshold. The energy levels measured from the $^6\text{He}+t$ threshold energy are shown in Fig. 2. The developed $^6\text{He}+t$ cluster states are suggested at the energy region a few MeV higher than the $^6\text{He}+t$ threshold energy. The $1/2_2^-$, $3/2_3^-$, $5/2_2^-$, and $7/2_2^-$ states are considered to be members of a $K^\pi = 1/2^-$ band which shows rather strong in-band $E2$ transitions due to the developed cluster structure (see Table I). The intrinsic wave functions of these states contain dominant components of the configuration (d) at $d = 5$ fm, and also significant components of the configuration (a) at $d = 5$ fm. The overlap of the $3/2_3^-$ state with $P_{M,K=1/2}^{J=3/2,-}\Phi_{(d)}(d = 5 \text{ fm})$ is 65% and, that with $P_{M,K=1/2}^{J=3/2,-}\Phi_{(a)}(d = 5 \text{ fm})$ is 45 %. As shown in Fig. 3 for the density distributions of the intrinsic wave functions, $\Phi_{(a)}(d = 5 \text{ fm})$ and $\Phi_{(d)}(d = 5 \text{ fm})$, the configuration (a) has the strong coupling feature where the t cluster is sitting on the head of the deformed ^6He cluster showing the elongate neutron structure, while the configuration (d) shows a characteristic of the weak coupling feature. Thus, the structure of the $K^\pi = 1/2^-$ band is regarded as the $^6\text{He}+t$ cluster structure with the intermediate feature between the strong coupling and the weak coupling regimes.

As we increase the model space by adding basis wave functions with larger d values, the energies of these states

above the $^6\text{He}+t$ cluster threshold decrease because of coupling with continuum states. It means that the GCM calculation within the $d = 1, 2, \dots, 8$ fm model space corresponds to a bound state approximation. We will discuss the stability of these resonance states later.

We also calculate ^{10}Be energy levels with the $^6\text{He}+^4\text{He}$ -cluster GCM calculations using the parameter $d = 1, 2, \dots, 8$ fm. The calculated energy and the $^6\text{He}+\alpha$ threshold energy are -56.9 and -46.8 MeV. As well as the case of ^9Li , they overestimate the experimental energy (-65.0 MeV) and threshold energy (-57.6 MeV). As shown in Fig. 4, the calculations reasonably reproduce the experimental energy spectra for the 0_1^+ , 2_1^+ , 2_2^+ , 0_2^+ , and 2_3^+ states in ^{10}Be . The $K^\pi = 0_2^+$ band near the $^6\text{He}+^4\text{He}$ threshold corresponds to the experimental 0_2^+ , and 2_3^+ states. The energies measured from the $^6\text{He}+^4\text{He}$ threshold are slightly underestimated by the calculations. The intrinsic structure of the $K^\pi = 0_2^+$ band shows a developed $^6\text{He}+^4\text{He}$ -cluster structure. The 0_2^+ state is dominated by the configurations (a) and (d) at $d = 5$ fm, each of which has about 70% overlap with the 0_2^+ state wave function. The remarkable component of the configuration (a) is consistent with the molecular orbital structure with the σ^2 molecular orbital configuration of the $K^\pi = 0_2^+$ band suggested by preceding works.

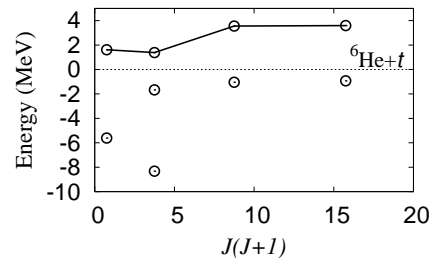


FIG. 2: Energy levels of negative-parity states in ^9Li calculated by the $^6\text{He}+t$ -cluster GCM method with $d = 1, 2, \dots, 8$ fm. Energies are measured from the $^6\text{He}+t$ threshold energy. Open circles connected by the solid line are $K^\pi = 1/2^-$ band members.

TABLE I: $E2$ transition strengths in ^9Li . The calculated transitions having $B(E2) \geq 1.0 \text{ e}^2\text{fm}^4$ are listed.

	$B(E2) (\text{e}^2\text{fm}^4)$
$3/2_1^- \rightarrow 1/2_1^-$	4.1
$3/2_3^- \rightarrow 1/2_2^-$	31
$5/2_2^- \rightarrow 1/2_2^-$	15
$5/2_1^- \rightarrow 3/2_2^-$	5.6
$5/2_2^- \rightarrow 3/2_3^-$	3.1
$7/2_1^- \rightarrow 3/2_1^-$	1.7
$7/2_2^- \rightarrow 3/2_3^-$	26
$7/2_2^- \rightarrow 5/2_2^-$	1.1

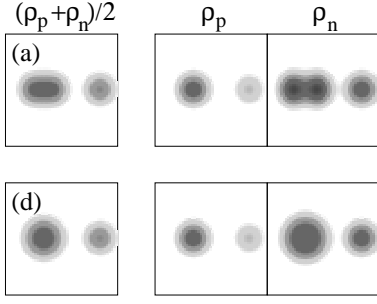


FIG. 3: Density distributions of the BB ${}^6\text{He}+t$ -cluster wave functions with the configuration (a) and (d) at $d = 5$ fm, $\Phi_{(a)}(d = 5 \text{ fm})$ and $\Phi_{(d)}(d = 5 \text{ fm})$. Distributions of the matter, proton and neutron density are shown left, middle and right, respectively.

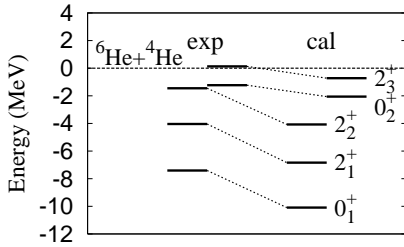


FIG. 4: Energy levels of positive-parity states in ${}^{10}\text{Be}$ obtained by the ${}^6\text{He}+{}^4\text{He}$ -cluster GCM calculations with $d = 1, 2, \dots, 8$ fm. The experimental energy levels for the corresponding states are also shown. Energies are measured from the ${}^6\text{He}+{}^4\text{He}$ threshold energy.

C. ${}^6\text{He}+t$ resonances above the threshold

In the previous subsection, we truncated the distance parameter as $d \leq 8$ and calculated energy levels within the bound state approximation. However, strictly speaking, the cluster states above the ${}^6\text{He}+t$ threshold energy can decay into the ${}^6\text{He}+t$ channel, and these ${}^6\text{He}+t$ resonance states couple with continuum states if we adopt an enough large model space for the inter-cluster distance. In fact, in the GCM calculation, energies and wave functions for the states above the threshold do not converge with respect to the model space of the generator coordinate d . As we increase the model space by adding basis wave functions with large d values, the energies of the states above the ${}^6\text{He}+t$ threshold decrease because of coupling with continuum states. We here discuss how the ${}^6\text{He}+t$ cluster states in the $K^\pi = 1/2^-$ band couple with continuum states.

To see the coupling with continuum states, we analyze the GCM calculation obtained with a larger model space of the distance $d = 1, 2, \dots, 15$ fm by using a pseudo potential method. We show in Appendix A applicability of an analysis with the pseudo potential method to the 2^+ resonance in α - α system. Usually, a pseudo potential is

used in the Analytic Continuation in the Coupling Constant (ACCC) method [29–32] to evaluate a complex energy pole for a resonance state. For the ACCC method, a high accuracy of the energy levels is required. However, in the present case, it is difficult to apply the ACCC method because the level crossing is complicated and the accuracy of the calculated energies is not enough for the analytic continuation. Therefore, we propose an alternative way for analysis.

We superpose ${}^6\text{He}+t$ cluster wave functions with $d = 1, 2, \dots, 15$ fm in Eq. 8. In the diagonalization of the Hamiltonian matrix, we introduce a pseudo potential and add it to the original Hamiltonian,

$$\tilde{H}(\delta) = H + \delta \times V^{\text{pseudo}} \quad (10)$$

$$V^{\text{pseudo}} = \sum_{i < j} v_0 \exp\left[-\frac{r_{ij}^2}{a_0^2}\right], \quad (11)$$

where $v_0 = -300$ MeV and $a_0 = 1.0$ fm are used. By diagonalizing the norm and Hamiltonian matrices with respect to \tilde{H} , we obtain the k th eigen energy $E_{6\text{He}+t}^{J_k^\pm}(\delta)$ and the eigen state,

$$|\tilde{\Psi}_M^{J_k^\pm}(\delta)\rangle = \sum_d \sum_{\alpha, K} \tilde{c}_{d, \alpha, K}^{(k)} P_{MK}^{J_k^\pm} |\Phi_\alpha(d)\rangle, \quad (12)$$

as functions of the strength δ of the pseudo potential. When $\delta = 0$, \tilde{H} equals to H . With increase of the strength δ of the pseudo potential, i.e., increase of the short-range two-body attraction added artificially, relative energies of resonance states to the ${}^6\text{He}+t$ threshold come down and finally become lower than the threshold energy. It means that, when the pseudo potential is strong enough, resonance states decouple from continuum states and change to bound states, which we call “pseudo bound states” in this paper.

Figure 5 shows energies of negative-parity states with the pseudo potential. The energies are measured from the ${}^6\text{He}+t$ threshold energy,

$$E^{J_k^-}(\delta) = E_{6\text{He}+t}^{J_k^-}(\delta) - E_{6\text{He}}(\delta) - E_t(\delta), \quad (13)$$

and are plotted as a function of the strength δ of the pseudo potential. As mentioned before, the $K^\pi = 1/2^-$ band is characterized by the significant component of the configuration (a) at $d = 5$ fm having a largely deformed neutron structure. For an enough strength δ of the pseudo potential, we can easily identify the $K^\pi = 1/2^-$ members which are specified by remarkable $P_{MK}^{J_k^-} \Phi_{(a)}(d = 5 \text{ fm})$ components. The energy curves for the identified states, are pointed by arrows in Fig. 5. We choose $\tilde{\Psi}^{1/2^-}(\delta = 0.12)$, $\tilde{\Psi}^{3/2^-}(\delta = 0.07)$, $\tilde{\Psi}^{5/2^-}(\delta = 0.16)$, and $\tilde{\Psi}^{7/2^-}(\delta = 0.15)$ as the pseudo bound states for the $K^\pi = 1/2^-$ band members following the criterion that $E^{J_k^-}(\delta) < 0$ and the states are decoupled from other states. As δ decreases, the energies of the ${}^6\text{He}+t$ cluster states go up while crossing continuum states. At $\delta = 0$ for the original Hamiltonian, the ${}^6\text{He}+t$ resonance

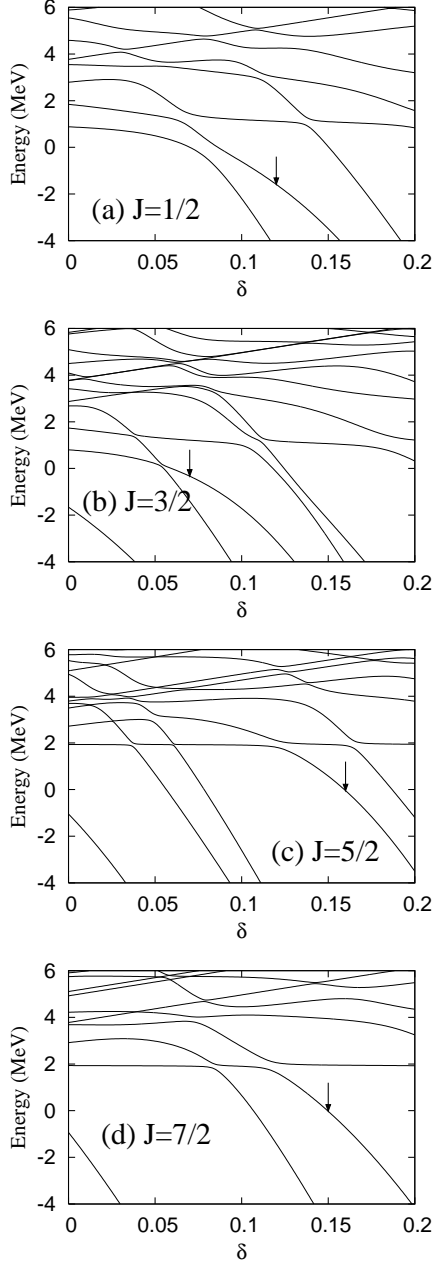


FIG. 5: Energies obtained by the ${}^6\text{He}+t$ -cluster GCM calculations with $d = 1, 2, \dots, 15$ fm using the pseudo potential. The energies measured from the ${}^6\text{He}+t$ threshold energy are plotted as a function of the strength δ .

states couple with continuum states and they are not distinguishable except for the $3/2^-$ state.

To evaluate energy spectra of the resonance states embedded in continuum states we analyze the overlaps of the pseudo bound states $\tilde{\Psi}^{J-}(\delta)$ for the $K^\pi = 1/2^-$ band members at the finite δ values selected above with the wave functions Ψ^{J_k-} of energy levels at $\delta = 0$. The amplitudes $|\langle \Psi^{J_k-} | \tilde{\Psi}^{J-}(\delta) \rangle|^2$ indicate how the pseudo bound states $\tilde{\Psi}^{J-}(\delta)$ for the ${}^6\text{He}+t$ cluster states fragments into

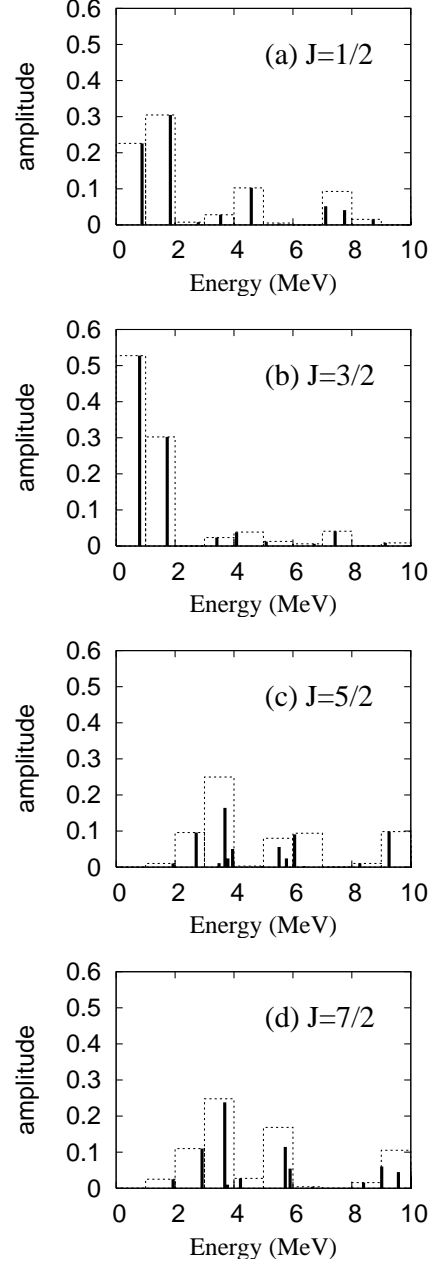


FIG. 6: Solid lines: distribution of the amplitudes $|\langle \Psi^{J_k-} | \tilde{\Psi}^{J-}(\delta) \rangle|^2$ for the ${}^6\text{He}+t$ cluster states in ${}^9\text{Li}$. For the pseudo bound states $\tilde{\Psi}^{J-}(\delta)$ for the ${}^6\text{He}+t$ cluster states in the $K^\pi = 1/2^-$ band, $\tilde{\Psi}^{1/2-}(\delta = 0.12)$, $\tilde{\Psi}^{3/2-}(\delta = 0.07)$, $\tilde{\Psi}^{5/2-}(\delta = 0.16)$, and $\tilde{\Psi}^{7/2-}(\delta = 0.15)$ are chosen. Histograms: sum of amplitudes in each energy intervals.

spectra at $\delta = 0$. The fragmentation of the amplitudes in the energy spectra may give information of resonance widths, because it may correspond to approximated spectra of the resonance states as shown in Appendix A

The distribution of the amplitudes is shown in Fig. 6. It is found that the amplitudes of the $1/2^-$ and $3/2^-$ states concentrate in the $0 \leq E \leq 2$ MeV region while

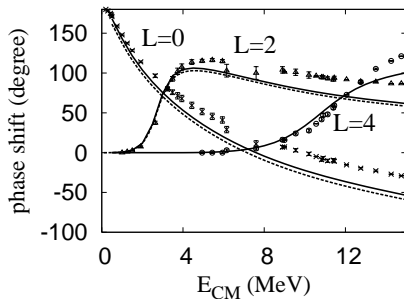


FIG. 7: α - α scattering phase shift calculated by using the Volkov No.2 force with $m = 0.60$. The solid and dashed lines indicate the phase shift obtained by 2α -cluster RGM calculations with the width parameter $\nu = 0.25 \text{ fm}^{-2}$ and $\nu = 0.235 \text{ fm}^{-2}$, respectively. Points are experimental data.

those of the $5/2^-$ and $7/2^-$ states are scattering in a wide energy region. These results suggest that widths of the $3/2^-$ and $1/2^-$ resonances may be of 1 MeV order, while those of the $5/2^-$ and $7/2^-$ states are expected to be larger than the $1/2^-$ and $3/2^-$ widths.

IV. SUMMARY

${}^6\text{He}+t$ cluster states in ${}^9\text{Li}$ were investigated by the ${}^6\text{He}+t$ -cluster GCM calculation. In the bound state approximation, the ${}^6\text{He}+t$ cluster states above the ${}^6\text{He}+t$ threshold energy are suggested. These states may construct a $K^\pi = 1/2^-$ band. They have an intermediate feature between the weak coupling cluster and strong coupling cluster regimes. In the strong coupling regime, the states show a largely deformed neutron structure with the configuration similar to the $K^\pi = 0_2^+$ band of ${}^{10}\text{Be}$.

We discussed resonance features of the ${}^6\text{He}+t$ cluster states by analyzing the results using a pseudo potential. Amplitudes of the $1/2^-$ and $3/2^-$ states in the energy spectra concentrate in the low-energy region, while those of the $5/2^-$ and $7/2^-$ states fragment widely.

Appendix A: Description of resonance state ${}^8\text{Be}(2^+)$ in an $\alpha+\alpha$ model

Two-body cluster states above the threshold energy are resonance states. When we superpose a finite number of BB wave functions without asymptotic outgoing wave boundary conditions, resonance states couple with continuum states if the model space of the distance parameter d is large enough. To see the coupling with continuum states in energy spectra, we analyze results of GCM calculations by using a pseudo potential method.

Let us consider here the 2^+ resonance in α - α system. In ${}^8\text{Be}$, the 2^+ state with a width 1.51 MeV is known at 3.12 MeV from the threshold energy. To show the applicability of the present analysis with the pseudo potential

method, we apply it to the α - α resonance.

We superpose fifteen BB $\alpha+\alpha$ cluster wave functions at $d = 1, 2, \dots, 15 \text{ fm}$ in the GCM calculation. In the diagonalization of the Hamiltonian matrix, we introduce the pseudo potential and add it to the original Hamiltonian H as explained in Eq. 10. The effective interaction used in the present work is the Volkov No.2 force with $m = 0.60$, which reproduces well the experimental data of α - α scattering phase shift as shown in Fig. 7. The width parameter ν is chosen to be $\nu = 0.235 \text{ fm}^{-2}$, which is the same value as that used for the ${}^6\text{He}+t$ and ${}^6\text{He}+\alpha$ calculations in the present work.

By diagonalizing the norm and Hamiltonian matrices with respect to \tilde{H} , we obtain the k th eigen energy $E_{2\alpha}^{Jk\pm}(\delta)$ and the eigen state $|\tilde{\Psi}_M^{Jk\pm}(\delta)\rangle$ as functions of the strength δ of the pseudo potential. Figure 8 shows the 2^+ state energies $E^{2k+}(\delta)$ which are measured from the threshold energy,

$$E^{2k+}(\delta) = E_{2\alpha}^{2k+}(\delta) - 2E_\alpha(\delta). \quad (\text{A1})$$

At $\delta = 0$, the resonance 2^+ state is obtained as the second 2^+ state at around 3 MeV. With increase of the strength δ of the pseudo potential, i.e., increase of the short-range two-body attraction added by hand, the energy for the resonance decreases, and it becomes lower than the threshold energy at $\delta = 0.13$.

To evaluate the energy spectra of the resonance state we see the amplitudes of the pseudo bound state wave function for the 2^+ state obtained at $\delta = 0.13$ in the energy levels at $\delta = 0$. The amplitudes $|\langle\Psi^{2k+}|\tilde{\Psi}^{2+}(\delta = 0.13)\rangle|^2$ indicate how the 2^+ resonance state fragments into energy spectra at $\delta = 0$. The fragmentation of the amplitudes is shown in Fig. 9 compared with the Breit-Wigner distributions given by the experimental energy position 3.12 MeV and the width 1.51 MeV for the ${}^8\text{Be}(2^+)$ state. The calculated distribution of the amplitudes seems to correspond well to the Breit-Wigner distribution. This result may suggest that the amplitudes calculated by the present method using the pseudo potential is useful to evaluate the energy and spectra of resonance states.

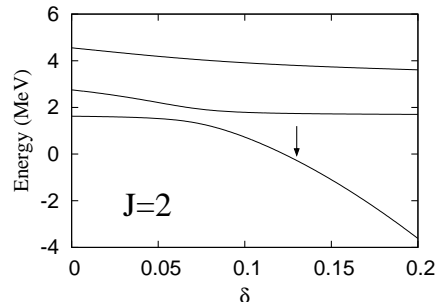


FIG. 8: Energies of 2^+ states obtained by the 2α -cluster GCM calculations with $d = 1, 2, \dots, 15 \text{ fm}$ using the pseudo potential. The energies measured from the 2α threshold energy are plotted as a function of the strength δ .

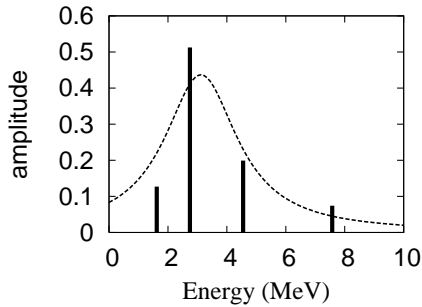


FIG. 9: Solid lines: distribution of the amplitudes $|\langle \Psi^{J_k-} | \tilde{\Psi}^{J-}(\delta) \rangle|^2$ for the 2^+ resonance in ^8Be . For the pseudo bound state, the wave function $\tilde{\Psi}^{J-}(\delta)$ obtained at $\delta = 0.13$ is chosen. Dashed line: Breit-Wigner distribution with the experimental energy position 3.12 MeV and width 1.51 MeV.

Acknowledgments

The computational calculations of this work were performed by using the supercomputers at YITP and done in Supercomputer Projects of High Energy Accelerator Research Organization (KEK). This work was supported by Grant-in-Aid for Scientific Research from Japan Society for the Promotion of Science (JSPS). It was also supported by the Grant-in-Aid for the Global COE Program "The Next Generation of Physics, Spun from Universality and Emergence" from the Ministry of Education, Culture, Sports, Science and Technology (MEXT) of Japan.

-
- [1] S. Okabe, Y. Abe, and H. Tanaka, Prog. Theory. Phys. **57**, 866 (1977); S. Okabe and Y. Abe, Prog. Theor. Phys. **59**, 315 (1978); S. Okabe, Y. Abe, Prog. Theory. Phys. **61**, 1049 (1979).
 - [2] M. Seya, M. Kohno, and S. Nagata, Prog. Theor. Phys. **65**, 204 (1981).
 - [3] W. von Oertzen, Z. Phys. A **354**, 37 (1996); **357**, 355 (1997).
 - [4] W. von Oertzen, Nuovo Cimento **110**, 895 (1997).
 - [5] K. Arai, Y. Ogawa, Y. Suzuki and K. Varga, Phys. Rev. C **54**, 132 (1996).
 - [6] A. Dote, H. Horiuchi and Y. Kanada-En'yo, Phys. Rev. C **56**, 1844 (1997).
 - [7] Y. Kanada-En'yo, H. Horiuchi and A. Doté, Phys. Rev. C **60**, 064304 (1999).
 - [8] N. Itagaki and S. Okabe, Phys. Rev. C **61**, 044306 (2000); N. Itagaki, S. Okabe and K. Ikeda, Phys. Rev. C **62**, 034301 (2000).
 - [9] Y. Ogawa, K. Arai, Y. Suzuki and K. Varga, Nucl. Phys. **A673**, 122 (2000).
 - [10] K. Arai, Y. Ogawa, Y. Suzuki, and K. Varga, Prog. Theor. Phys. Suppl. **142**, 97 (2001).
 - [11] Y. Kanada-En'yo M. Kimura and H. Horiuchi, C. R. Physique **4** 497 (2003).
 - [12] Y. Kanada-En'yo and H. Horiuchi, Phys. Rev. C **68**, 014319 (2003).
 - [13] W. von Oertzen, M. Freer and Y. Kanada-En'yo, Phys. Rep. **432**, 43 (2006).
 - [14] M. Freer, *et al.*, Phys. Rev. Lett. **82**, 1383 (1999); M. Freer, *et al.*, Phys. Rev. C **63**, 034301 (2001).
 - [15] A. Saito, *et al.*, Nucl. Phys. **A738**, 337 (2004).
 - [16] N. Curtis *et al.*, Phys. Rev. C **70**, 014305 (2004).
 - [17] H. G. Bohlen, T. Dorsch, T. Kokalova, W. von Oertzen, C. Schulz and C. Wheldon, Phys. Rev. C **75**, 054604 (2007).
 - [18] M. Ito, K. Kato and K. Ikeda, Phys. Lett. B **588**, 43 (2004).
 - [19] K. Arai, Phys. Rev. C **69**, 014309 (2004).
 - [20] M. Ito, N. Itagaki, H. Sakurai and K. Ikeda, Phys. Rev. Lett. **100**, 182502 (2008).
 - [21] Y. Kanada-En'yo, Phys. Rev. C **66**, 011303 (2002).
 - [22] K. Ikeda, N. Tagikawa, and H. Horiuchi, Prog. Theor. Phys. Suppl. extra number, 464 (1968).
 - [23] T. Suhara and Y. Kanada-En'yo, Prog. Theor. Phys. **123**, 303 (2010).
 - [24] D. M. Brink, International School of Physics "Enrico Fermi", XXXVI, p. 247 (1966).
 - [25] Y. Kanada-En'yo, H. Horiuchi and A. Ono, Phys. Rev. C **52**, 628 (1995); Y. Kanada-En'yo and H. Horiuchi, Phys. Rev. C **52**, 647 (1995).
 - [26] A. B. Volkov, Nucl. Phys **74**, 33 (1965).
 - [27] N. Yamaguchi, T. Kasahara, S. Nagata and Y. Akaishi, Prog. Theor. Phys. **62**, 1018 (1979); R. Tamagaki, Prog. Theor. Phys. **39**, 91 (1968).
 - [28] T. Suhara and Y. Kanada-En'yo, Phys. Rev. C **82**, 044301 (2010).
 - [29] V. I. Kukulin and V. M. Krasnopol'sky, J. Phys. A **10**, 33 (1977); V. I. Kukulin, V. M. Krasnopol'sky, and M. Miskhi, Sov. J. Nucl. Phys. **29**, 421 (1979).
 - [30] N. Tanaka, Y. Suzuki, K. Varga and R. G. Lovas, Phys. Rev. C **59**, 1391 (1999).
 - [31] S. Aoyama, Phys. Rev. C **68**, 034313 (2003).
 - [32] Y. Funaki, H. Horiuchi and A. Tohsaki, Prog. Theor. Phys. **115**, 115 (2006).